Parametric Analysis of Cooling Properties of Candidate Expander-Cycle Fuels

Annafederica Urbano, Francesco Nasuti

▶ **To cite this version:**

Annafederica Urbano, Francesco Nasuti. Parametric Analysis of Cooling Properties of Candidate Expander-Cycle Fuels. Journal of Propulsion and Power, 2014, 30 (1), pp.153-163. 10.2514/1.B34852 . hal-03318270

HAL Id: hal-03318270
https://hal.science/hal-03318270

Submitted on 9 Aug 2021

HAL is a multi-disciplinary open access archive for the deposit and dissemination of scientific research documents, whether they are published or not. The documents may come from teaching and research institutions in France or abroad, or from public or private research centers.

L'archive ouverte pluridisciplinaire **HAL**, est destinée au dépôt et à la diffusion de documents scientifiques de niveau recherche, publiés ou non, émanant des établissements d'enseignement et de recherche français ou étrangers, des laboratoires publics ou privés.

Open Archive Toulouse Archive Ouverte (OATAO)

OATAO is an open access repository that collects the work of some Toulouse researchers and makes it freely available over the web where possible.

This is an author's version published in: https://oatao.univ-toulouse.fr/27980

Official URL: https://doi.org/10.2514/1.B34852

To cite this version :

Urbano, Annafederica and Nasuti, Francesco Parametric Analysis of Cooling Properties of Candidate Expander-Cycle Fuels. (2014) Journal of Propulsion and Power, 30 (1). 153-163. ISSN 0748-4658

Any correspondence concerning this service should be sent to the repository administrator:
tech-oatao@listes-diff.inp-toulouse.fr

Parametric Analysis of Cooling Properties of Candidate Expander-Cycle Fuels

Annafederica Urbano* and Francesco Nasuti†
University of Rome "La Sapienza," 00184 Rome, Italy

DOI: 10.2514/1.B34852

Flow evolution and heat transfer capability in the cooling system of liquid rocket engines heavily depend on propellant thermophysical properties. Coolant thermophysical property analysis and modeling is therefore important to study the possibility of relying on a regenerative cooling system, whose performance is crucial to determine feasibility and convenience of pump-fed liquid rocket cycles of the expander type. The aim of the present study is to compare the behavior of different liquid fuels for expander-cycle engines. They are light hydrocarbons, binary mixtures of them, and liquefied natural gas, which is a mixture made basically of methane and minor fractions of other light hydrocarbons and nitrogen. A parametric analysis is carried out by a validated numerical solver to compare temperature increase, pressure loss, and heat transfer evolution for the different fuels along the same straight tube and subjected to assigned heat fluxes. Results show that similar engine performance can be obtained by the different candidate expander-cycle fuels, but significant differences can be seen in the flow evolution through the cooling channels.

Nomenclature

A	=	Helmholtz free energy, J/kg
a	=	reduced Helmholtz free energy, $a = A/(RT)$
c_p	=	specific heat at constant pressure, $\mathrm{J/(kg \cdot K)}$
D	=	channel cross section diameter, m
$\mathbf{F_e}$	=	parabolized vector of Eulerian fluxes in the streamwise direction
G	=	specific mass flow rate, $\mathrm{kg/(s \cdot m^2)}$
$\mathbf{G_e}$, $\mathbf{H_e}$	=	vectors of Eulerian fluxes in the transverse directions
$\mathbf{G_v}$, $\mathbf{H_v}$	=	vectors of viscous fluxes in the transverse directions
h	=	enthalpy, J/kg
h_c	=	heat transfer coefficient, $\mathrm{W/(K \cdot m^2)}$
k	=	thermal conductivity, $\mathrm{W/(m \cdot K)}$
O/F	=	oxidizer-to-fuel mass ratio
$\mathbf{P}$	=	pressure term vector for parabolized Navier–Stokes equations
p	=	pressure, Pa
$\mathbf{Q}$	=	source terms vector
Q	=	heat transfer rate, W
q	=	heat flux, $\mathrm{W/m^2}$
R	=	gas constant, $\mathrm{J/(kg \cdot K)}$
r	=	nozzle radius, m
T	=	temperature, K
u	=	streamwise velocity component, m/s
u_{eq}	=	equivalent exhaust velocity, m/s
v, w	=	transverse velocity components, m/s
x	=	streamwise direction and coordinate
$\bar{x}$	=	vector of molar fractions
y, z	=	transverse directions and coordinates
Z	=	compressibility factor, $Z = p/(\rho RT)$
δ	=	reduced density ρ/ρ_{cr}
ε	=	area ratio
Λ	=	generic transport property
μ	=	viscosity, $\mathrm{Pa \cdot s}$
ρ	=	density, $\mathrm{kg/m^3}$
τ	=	reduced temperature T_{cr}/T

Subscripts

b	=	bulk value
cc	=	combustion chamber
cr	=	critical value
ev	=	boiling value
ex	=	excess property
id	=	perfect gas term
in	=	inlet
max	=	maximum value
pc	=	pseudocritical value
r	=	reducing value
ref	=	reference species
st	=	stoichiometric value
t	=	turbine
th	=	nozzle throat
w	=	wall
0	=	total
$1, \ldots, 5$	=	first, . . . , fifth component of flux vectors

Superscripts

r	=	residual term
0	=	perfect gas term
*	=	selected value

I. Introduction

TOPPING systems provide the most efficient solution for thermodynamic power cycles of turbopump-fed liquid rocket engines [1,2]. Among them, the expander cycle is the simplest and has been considered the best solution when moderate chamber pressure and restartability are the parameters of interest. The typical application for this cycle is therefore that of upper stages. In expander cycles, gas turbine power is obtained from available coolant enthalpy, which is captured from the cooling system. Therefore, engine performance is strictly connected with the coolant thermophysical properties and with its heat transfer characteristics in heated channels. Possible coolant candidates which, at least theoretically, make the system feasible with satisfying performance requirements are fuels like hydrogen, methane, and propane [1]. These liquid propellants flow in cooling channels at supercritical pressures. In particular,

*Ph.D., Research Fellow, Dipartimento di Ingegneria Meccanica e Aerospaziale, Via Eudossiana 18. Student Member AIAA.
†Associate Professor, Dipartimento di Ingegneria Meccanica e Aerospaziale, Via Eudossiana 18. Associate Fellow AIAA.

Table 1 Main properties of expander-cycle fuel candidates with RP-1 data provided for comparison

Fuel	T_{cr}, K	p_{cr}, bar	T_{ev}, K	T_{max}, K [12,13]	ρ, kg/m^3	$(O/F)_{st}$	$(O/F)^*$
H_2	33	12.9	20	978	71.0	8.00	5.50
CH_4	190	46.0	112	978	422.6	4.00	2.85
C_2H_6	305	48.7	184	778	546.5	3.73	2.55
C_3H_8	370	42.5	231	733	582.0	3.63	2.50
RP-1, $C_nH_{1.953n}$	679	23.4	493	561	820.0	3.41	2.35

hydrocarbons, which have a higher critical pressure than hydrogen, for a same operative pressure would be closer to critical pressure than hydrogen and thus could flow in channels at a near-critical pressure. In such conditions, thermophysical properties are subject to great variations, which could affect, locally, the heat transfer capabilities of the propellants. The main goal of the present study is to compare the behavior of different light hydrocarbons and their mixtures flowing in the cooling channels of an expander-cycle engine. Attention is also devoted to typical liquefied natural gas (LNG) mixtures. In fact, commercial LNG contains about 90% or more methane in a mixture including ethane, propane, butane, and nitrogen in different percentages for the remaining part. To obtain pure methane, LNG must be further processed, with an obvious increase in propellant cost. The cheaper LNG has therefore been considered as a possible rocket engine fuel instead of pure methane [3–5].

In the present study, the parametric investigation on the behavior of different fuels and fuel mixtures in straight heated tubes has been carried out by a suitable numerical solver, able to manage the complex flow modeling and thermodynamic phenomena, which affect heat transfer to turbulent supercritical fluids. More specifically, a solver of parabolized Navier–Stokes equations [6] is used, where parabolization is obtained by neglecting viscous derivatives in the space-marching direction, while retaining crosswise derivatives, and by considering the streamwise pressure gradient as a source term evaluated on the basis of the overall momentum balance. The algorithm is based on a finite volume approach with a Godunov-type scheme, which uses a modified Roe's approximate Riemann solver for a fluid governed by a generic equation of state (EoS) [7]. Using parabolized Navier–Stokes equations (PNS) is particularly suitable for parametric analysis with a negligible loss of precision in physical modeling with respect to full Navier–Stokes solvers. Because of the near-critical expected fluid conditions of interest, appropriate EoS and transport property relations for real fluids and mixtures of real fluids are required. In particular, in the present study, the model of Groupe Européen de Recherches Gazières (GERG) [8] has been selected for the EoS, whereas the extended corresponding states (ECS) models of Huber et al. [9] and Klein et al. [10] have been used for the transport properties.

In the following, a comparative overview between the light hydrocarbons and hydrogen, when used in an expander cycle, is presented, both considering the thermophysical properties of the propellants and the predictable engine performance, considering oxygen as the oxidizer. Then the main details of numerical approach and the thermophysical property modeling are presented. Finally, the numerical simulations of the different candidate fuels flowing in straight heated channels are presented and compared. Discussion of results is focused on the total pressure losses and the cooling capabilities, which are the two main aspects to be considered when dealing with the regenerative system of expander-cycle engines.

II. Candidate Fuels for Expander-Cycle Engines

Only a limited number of rocket fuels are able to extract power from the liquid rocket engines (LRE) cooling system to drive the turbopump to get a significant chamber pressure increase. In the literature, only three liquid fuels have been considered as a viable option: hydrogen, methane, and propane. The reason is that a fuel compatible with expander cycles "must have a high heat capacity and adequate heat transfer properties, and it must vaporize easily" [1]. In fact, expander cycles are based on gas turbines, which require availability of "hot gas." However, if hot gas is available, the coolant can only reach temperatures lower than the maximum allowable structural temperature (about 800–1000 K), being the gas provided by heating the coolant in the cooling system. This limiting temperature can be even lower because of changes of fuel properties at high temperature (e.g., pyrolysis or thermal cracking and coking [11]). Therefore, there is a maximum power that can be theoretically extracted from the turbine due to the maximum allowable coolant temperature. Maximum coolant temperature for light hydrocarbons in a regenerative cooling system, due to either maximum allowable structural temperature (methane) or thermal decomposition, has been evaluated in [12,13] and is reported in Table 1, together with the main properties of candidate expander fuels. Also, Rocket Propellant-1 (RP-1) properties are reported for the sake of completeness. The latter is shown as a reference for rocket hydrocarbon fuels. In particular, Table 1 shows the critical temperature and pressure of fuels (T_{cr} and p_{cr}, respectively), the boiling point, the maximum coolant temperature, the liquid phase density, the stoichiometric oxidizer-to-fuel mass ratio $(O/F)_{st}$, and the value $(O/F)^*$ considered for the performance analysis in this study. Methane and hydrogen maximum temperature is that allowed by structural temperature, whereas for ethane, propane, and RP-1, the maximum temperature is limited by thermal decomposition. The qualitative evolution of fuels listed in Table 1 in an expander-cycle engine is shown in Fig. 1. Starting from the tank, where fuels are at low pressure and their temperature is close to the saturation line for cryogenic fuels, whereas it is quite lower for RP-1, the fluid evolves through the pump, increasing its pressure. In the figure, the increase of temperature due to losses in the pump is neglected for the sake of simplicity of the image. The candidate fuel, to be ready to pass to the gaseous phase without a phase change, has to reach a pressure larger than the critical pressure. Therefore, the minimum pressure to be reached downstream of the pump has been assumed as about 15% larger than the critical one (pump exit region). Next, the fuel has to flow through the cooling circuit to both cool the thrust chamber wall and get thermal energy to expand in turbine, at the cost of some pressure loss. Giving no particular emphasis to such pressure losses, here attention is focused on the increase of fuel temperature. Limits on temperature are those given in Table 1. In the figure, it is assumed that the fuel takes all the energy necessary to reach its maximum allowable

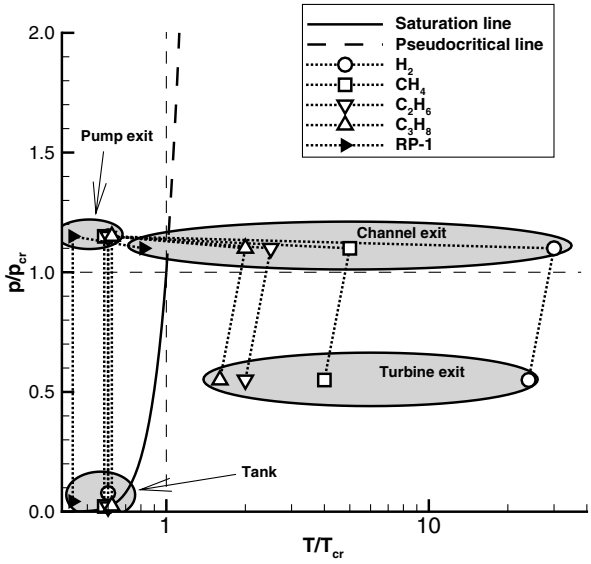

Fig. 1 Qualitative evolution of reduced temperature (T/T_{cr}) and pressure (p/p_{cr}) of selected fuels in a typical expander-cycle evolution. RP-1 data are shown for the sake of comparison.

temperature. It is interesting to note that, by increasing the fuel carbon content, the maximum reduced temperature moves left, toward the unity, up to reach a value lower than one ($T < T_{cr}$) for RP-1. This means that RP-1 reaches its maximum allowable temperature (561 K) when it is still in a liquid-like phase, and thus it is not able to exploit thermal energy in a turbine. Therefore, the RP-1 state at the turbine exit cannot be shown in the plot and, as known, RP-1 cannot be considered as an expander-cycle fuel candidate. On the contrary, hydrogen and the light hydrocarbons considered all show their possible use as expander-cycle fuels, terminating their cycle at the turbine exit in a gaseous phase, without passing for two-phase flow regions (turbine inlet/outlet pressure ratio has been assumed as about two). It is evident that hydrogen margins are quite different from the other fuels, however, methane, ethane, and propane show properties compatible with their use as expander-cycle fuels.

Engine performance can be studied by the vacuum specific impulse behavior, here presented as equivalent exhaust velocity u_{eq} (Fig. 2a). Curves presented in Fig. 2a have been obtained by CEA software [14,15] assuming chamber pressure $p_{cc} = 60$ bar, area ratio $\varepsilon = 100$, equilibrium expansion up to throat, and frozen expansion in the divergent section. Liquid oxygen is the only oxidizer considered. As well known, it can be seen that there is a maximum performance value in conditions rather far from stoichiometric. Stoichiometric conditions $(O/F) = (O/F)_{st}$ are emphasized with a triangle in Fig. 2a. The maximum values only refer to engine performance, whereas the overall system optimum performance would require larger (O/F) values because of the small storage density of fuels. Note that there is only a few percent difference on the maximum ideal performance of light hydrocarbons.

The foregoing performance can be obtained provided a certain chamber pressure level is reached. It is worthwhile, therefore, to make a gross estimation of the expected chamber pressure that can be obtained for the selected fuel candidates. The estimation is made by taking as a reference the RL-10A-4-1, a version of the RL-10A engine, which has about 50 years of flight heritage [16,17] and whose properties are known. In particular, chamber pressure is evaluated by power balances between turbine and oxidizer and fuel pumps, considering pressure losses in ducts proportional to channel pressure for the same factor as in RL-10A-4-1. The turbomachine efficiencies are also roughly estimated from RL-10A-4-1 values. Results for chamber pressure as a function of the maximum fuel pressure (just downstream of the fuel pump) for the selected $(O/F) = (O/F)^*$ are shown in Fig. 2b. A temperature of $T_t = 600$ K is assigned at the turbine inlet. Note that, typically for hydrogen, due to its high thermal capacity, there is not enough thermal power to extract to reach this value of T_t. This is quite a high temperature if hydrogen is considered as a fuel. Actually, practical examples of expander-cycle engines using hydrogen have a turbine inlet temperature around 200 K. For instance, points indicating the reference RL-10A-4-1 and the Vinci engines, having the former at turbine inlet $T_t = 211$ K, the latter $T_t = 240$ K, are also reported in Fig. 2b together with the curves relevant to these values of T_t. It can be noticed that all of the three light hydrocarbons studied here promise performance comparable to the present hydrogen expander cycle like RL-10A-4-1 and Vinci, provided that a higher turbine temperature is considered. It can also be seen that the values of chamber pressure obtained with hydrocarbons are quite close to each other, with a slight increase passing from methane to ethane and then to propane.

III. Numerical Model

Parametric analysis of channel flows can be successfully made resorting to the PNS equations which are an approximation of the complete set of Navier–Stokes equations. Such an approach is considered in the present study: In fact, parabolization assumptions can be made for the channel flows of the present investigation. The present in-house PNS solver developed by the authors has been validated against experimental data [6,18] in conditions similar to those that have to be analyzed. For the sake of completeness, an introduction of the numerical model is reported, and further details can be found in [6,7].

Considering a Cartesian reference system for a straight tube, if x is the streamwise direction and y and z are the transverse directions, the conservative form of the three-dimensional PNS equations is

$$\frac{\partial \mathbf{F_e}}{\partial x} + \frac{\partial \mathbf{G_e}}{\partial y} - \frac{\partial \mathbf{G_v}}{\partial y} + \frac{\partial \mathbf{H_e}}{\partial z} - \frac{\partial \mathbf{H_v}}{\partial z} = \frac{\partial \mathbf{P}}{\partial x} + \mathbf{Q} \tag{1}$$

where the subscripts e and v indicate the Eulerian and viscous flux vectors, respectively, after the PNS approximation has been applied. In particular, these equations have been obtained by neglecting the streamwise viscous flux vector and the x derivatives in the transverse viscous flux vectors (in $\mathbf{G_v}$ and $\mathbf{H_v}$ all the x derivatives have been neglected). Moreover, the streamwise pressure gradient is considered as a source term $\partial\mathbf{P}/\partial x$ and therefore pressure does not appear in the streamwise Eulerian flux $\mathbf{F_e}$. A further source term vector $\mathbf{Q}$ has been emphasized in Eq. (1) for the sake of generality. The resulting expressions of the flux vectors are

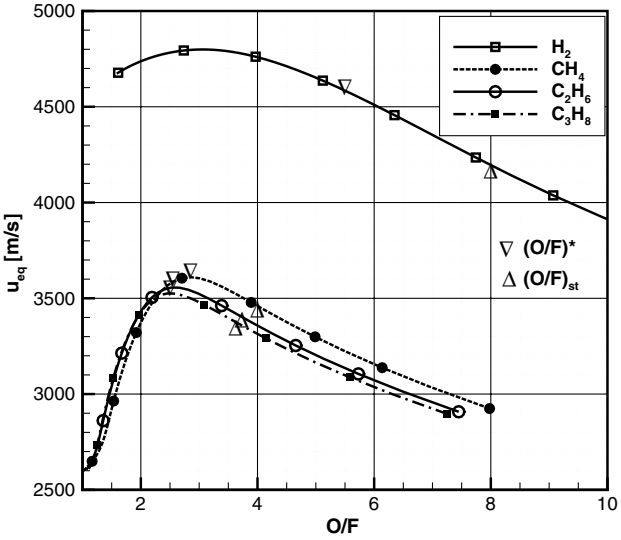

a) Equivalent exhaust velocity as a function of mixture ratio at $p_{cc} = 60$ bar

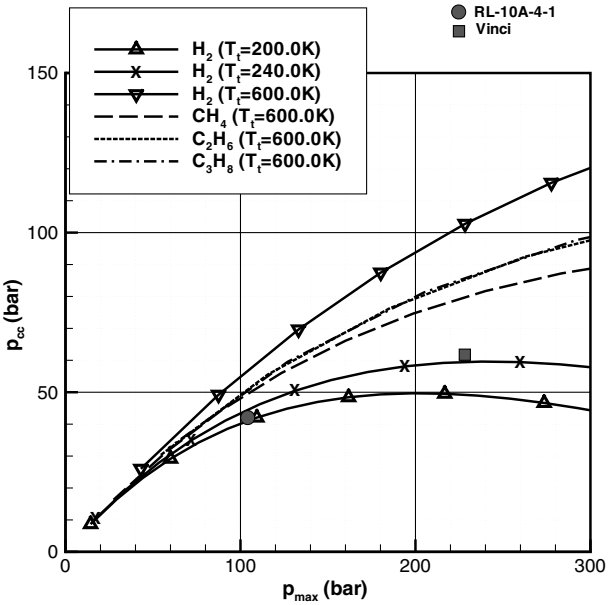

b) Chamber pressure vs fuel maximum pressure at $(O/F) = (O/F)^*$

Fig. 2 Performance analysis for candidate expander-cycle engine fuels and oxygen as oxidizer ($\varepsilon = 100$).

$$\mathbf{F}_e = \begin{Bmatrix} \rho u \\ \rho u^2 \\ \rho uv \\ \rho uw \\ \rho u h_0 \end{Bmatrix} \quad G_e = \begin{Bmatrix} \rho u \\ \rho uv \\ \rho v^2 + p \\ \rho uw \\ \rho v h_0 \end{Bmatrix} \quad \mathbf{H}_e = \begin{Bmatrix} \rho w \\ \rho uw \\ \rho vw \\ \rho w^2 + p \\ \rho w h_0 \end{Bmatrix} \tag{2}$$

$$\mathbf{G_v} = \begin{Bmatrix} 0 \\ \mu \dfrac{\partial u}{\partial y} \\ \frac{2}{3}\mu\left(2\frac{\partial v}{\partial y} - \frac{\partial w}{\partial z}\right) \\ \mu\left(\frac{\partial v}{\partial z} + \frac{\partial w}{\partial y}\right) \\ uG_{v,2} + vG_{v,3} + wG_{v,4} + k\frac{\partial T}{\partial y} \end{Bmatrix}$$

$$\mathbf{H_v} = \begin{Bmatrix} 0 \\ \mu \dfrac{\partial u}{\partial z} \\ \mu\left(\frac{\partial v}{\partial z} + \frac{\partial w}{\partial y}\right) \\ \frac{2}{3}\mu\left(2\frac{\partial w}{\partial z} - \frac{\partial v}{\partial y}\right) \\ uH_{v,2} + vH_{v,3} + wH_{v,4} + k\frac{\partial T}{\partial z} \end{Bmatrix} \tag{3}$$

where subscripts 2, 3, and 4, indicate the second, third, and fourth component of vectors, respectively.

Finally, the pressure source term is given by

$$\mathbf{P} = \begin{Bmatrix} 0 \\ -p \\ 0 \\ 0 \\ 0 \end{Bmatrix} \tag{4}$$

The Reynolds-averaged Navier–Stokes approach is considered to take into account turbulence. Closure is obtained by computation of eddy viscosity according to the one equation model of Spalart and Allmaras [19], modified to take into account the PNS hypothesis. The diffusion-convection equation for the turbulent viscosity is solved together with Eq. (1), in which viscosity μ and conductivity k include both molecular and turbulent contributions.

Considering that the system of equations is hyperbolic parabolic in the streamwise direction, the numerical solution of Eq. (1) can be obtained using a space-marching method. The present space-marching method relies on a finite volume scheme in which the unknown $\mathbf{F_e}$ fluxes are integrated in the x direction with an Euler explicit scheme once the $\mathbf{G_e}$, $\mathbf{G_v}$, $\mathbf{H_e}$, and $\mathbf{H_v}$ fluxes have been evaluated at the cell interfaces. The Riemann solver is a modified version of the Roe's approximate Riemann solver [20] for Eq. (1) with generic equations of state. Details on the Riemann solver can be found in [7].

To make this integration possible, the pressure source term has to be known. In fact, one of the critical aspects of the use of the PNS approach in channel flows is how to compute the streamwise pressure gradient, which has to be evaluated at each integration step. The assumed closure in the present approach is that of evaluating the $\partial\mathbf{P}/\partial x$ term in Eq. (1) with an iteration process, which finds the value of $\partial\mathbf{P}/\partial x$ such that the conservation of the integral momentum equation at each integration step along the channel length is satisfied [6].

IV. Thermophysical Property Models

A. Equation of State

The thermodynamic description of the propellant is particularly important in the frame of the present study, which aims to evaluate the influence of the thermophysical properties on the coolant behavior. Both pure fluids and mixtures of hydrocarbons are considered. Dealing with mixtures of hydrocarbons, the most recent and reliable equation of state is that presented in the GERG study [8], which has been built especially to describe natural gas mixtures. The GERG study is based on the Helmholtz free energy EoS, which takes into account the real behavior of fluids with some kind of departure function from the perfect gas. In particular, the GERG EoS is based on pure substance equation of state for each considered mixture component and correlation equations for binary mixtures consisting of these components. Mixing rules are applied to the reduced Helmholtz free energy a:

$$a(\delta, \tau, \bar{x}) = \frac{A}{RT} = a^0(\rho, T, \bar{x}) + a^r(\delta, \tau, \bar{x}) \tag{5}$$

with ρ and T being, respectively, the mixture density and temperature, R the gas constant, A the mass specific Helmholtz free energy, and $\bar{x} = (x_1, x_2, \ldots, x_N)$ the molar composition. The residual term a^r, which corrects in the real fluid regime the perfect gas term a^0, is expressed in terms of reduced mixture density δ and reduced mixture temperature τ, according to

$$\delta = \frac{\rho}{\rho_r(\bar{x})} \quad \text{and} \quad \tau = \frac{T_r(\bar{x})}{T} \tag{6}$$

The reducing parameters $\rho_r(\bar{x})$ and $T_r(\bar{x})$ are combinations of the critical parameters of the single species and reduce to the critical parameters for a pure fluid. Further details and the values of model coefficients can be found in [8,21]. The fundamental equation of state describing the Helmholtz free energy as a function of temperature and density, with its derivatives, is sufficient to provide a complete description of the thermodynamic properties of the mixture. Once the equation of state for the reduced Helmholtz free energy is available, the other thermodynamic properties of the mixture (compressibility factor, pressure, enthalpy, specific heats, etc.) can be obtained from its derivatives with respect to reduced temperature and density. The range of validity of GERG EoS covers temperatures in the range $60 \leq T \leq 700$ K and pressures lower than 70 MPa, with an uncertainty in density lower than 0.5%. For temperatures higher than 700 K, a perfect gas equation of state is considered, assuming that no pyrolysis occurs. Indeed, temperatures higher than 700 K are only considered in the present study to understand wall heating trends at high heat fluxes and to warn about possible unacceptable flow conditions like, for instance, those leading to hydrocarbon pyrolysis and coking [22]. An example of the constant pressure specific heat c_p of different hydrocarbons and their mixtures in the thermodynamic conditions of interest in the present study is shown in Fig. 3a.

B. Transport Properties

Excess property models have been used to describe the transport properties. Namely, if Λ is either the molecular viscosity μ or the molecular thermal conductivity k, the model has the following generic form:

$$\Lambda(\rho, T) = \Lambda_{\text{id}}(T) + \Lambda_{\text{ex}}(\rho, T) \tag{7}$$

where Λ_{ex} is the excess property from the dilute gas term Λ_{id}. For the dilute gas part, molecular viscosity and thermal conductivity expressions are taken from [14], according to literature empirical relations provided in [23,24]. The dependence of transport properties on temperature is in the form

$$\Lambda_{\text{id}}(T) = 10^{-7} \cdot \exp[a_{\Lambda,1}\,\log(T) + a_{\Lambda,2}T^{-1} + a_{\Lambda,3}T^{-2} + a_{\Lambda,4}] \tag{8}$$

where the coefficients $a_{\Lambda,i}$ can be found in [24]. Data for propane are not available in [23,24]. Hence, the dilute gas part of the viscosity model presented in [25] and of the thermal conductivity model presented in [26] have been considered to evaluate Λ_{id} for propane. Excess viscosity and conductivity have been evaluated using

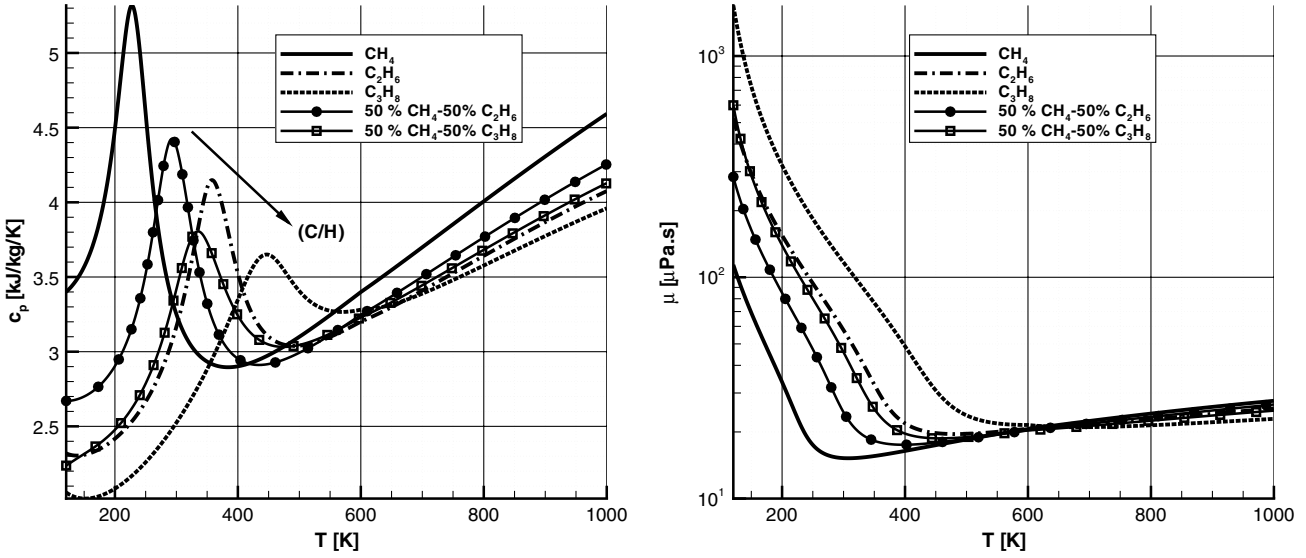

a) Specific heat at constant pressure **b) Molecular viscosity**

Fig. 3 Specific heat at constant pressure and molecular viscosity for methane, ethane, propane, and 50% binary mixtures propane–methane and ethane–methane, for $p = 13$ MPa.

different accurate correlations available in the literature for the considered species [25–30].

An excess property approach is also used to get mixture transport properties [21]. The ideal gas contribution is evaluated, combining single species properties with the mixture rules for perfect gas [14,23,24]. Excess properties are evaluated according to the ECS theory presented in [9,10]. Following this approach, viscosity and thermal conductivity are accurately evaluated for a reference fluid (which is nitrogen in the present study [31]). The basic assumption of the ECS model is that

$$\Lambda_{\text{ex}}(T,\rho,\bar{x}) = \Lambda_{\text{ex,ref}}(T_{\text{ref}},\rho_{\text{ref}})F^r_\Lambda \tag{9}$$

Specifically, the excess property of the mixture is equal to the excess property of the reference fluid $\Lambda^{\text{ex}}_{\text{ref}}$, evaluated at specific temperature and densities, the conformal temperature T_{ref} and density ρ_{ref}, and modified for a correction factor F^r_Λ. Assuming that the excess viscosity of the reference fluid as a function of temperature and density is known, it is only necessary to evaluate conformal temperature and density and the reducing factor F^r_Λ. The conformal temperature and density are defined such that

$$\begin{cases} a^r(T,\rho,\bar{x}) = a^r_{\text{ref}}(T_{\text{ref}},\rho_{\text{ref}}) \\ Z(T,\rho,\bar{x}) = Z_{\text{ref}}(T_{\text{ref}},\rho_{\text{ref}}) \end{cases} \tag{10}$$

where a^r is the residual part of the reduced Helmholtz free energy ($a = A/RT$), Z is the compressibility factor of the mixture, and a^r_{ref} and Z_{ref} are the corresponding functions for the reference fluid. For the conductivity, a further contribution is included due to the critical enhancement [32]. An example of the molecular viscosity of different hydrocarbons and their mixtures in the thermodynamic conditions of interest in the present study is shown in Fig. 3b.

V. Geometry and Boundary Conditions

To compare the cooling behavior of propellants with each other, different numerical simulations have been carried out on a two-dimensional axisymmetric geometry, which is a straight channel with a circular cross section of diameter $D = 4$ mm. In Fig. 4, a schematic of the test case with the enforced boundary conditions is shown. In the first 100 diameters, no heat flux is applied, whereas a constant heat flux q_w of 5 or 7 MW/m^2 is enforced from $x/D = 100$ to the end of the channel. Specifically, in the present finite volume approach, the heat flux is directly enforced, assigning the value of the last component of $\mathbf{G_v}$, and the wall temperature is inferred from the wall heat flux and the flowfield solution. The selected heat flux values are of the order of magnitude of those expected in expander-cycle engines once they are rescaled to preserve the heat input in each channel and once input heat flux to the channel is assumed to be axisymmetric. In actual engines, the peak heat flux can be one order of magnitude higher but it only acts on the channel side wet by hot gases. In fact, if one considers the heat input Q exiting an axisymmetric thrust chamber in the throat region over a length dx in the axial direction

$$Q = 2\pi r_{\text{th}} q_{\text{th}} dx \tag{11}$$

and considers that this heat is distributed to N channels, the average axisymmetric wall heat flux entering each channel must satisfy the balance

$$q_w = \frac{Q/N}{\pi D dx} = q_{\text{th}} \frac{2r_{\text{th}}}{ND} \tag{12}$$

It is easy to see that, considering values of the order of magnitude of those known for engines of the RL-10-A family ($N = 100$–200,

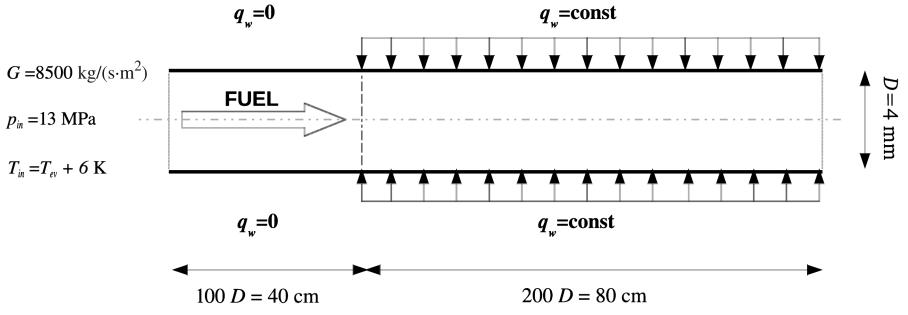

Fig. 4 Schematic of the computational domain with the enforced boundary conditions (not to scale).

$D = 3$–4 mm, and $r_{\text{th}} = 30$–40 mm), the scaling factor q_w/q_{th} is 0.1–0.2 [33]. The entrance adiabatic length is needed to obtain a developed flow before heating. For each heat flux level, the parametric study has been carried out for a same specific mass flow rate $G = 8500\ \text{kg}/(\text{s} \cdot \text{m}^2)$ and inlet pressure $p_{\text{in}} = 13$ MPa. On the other hand, a different inlet temperature is assigned for each species or mixture of species. In fact, both the geometry and the boundary conditions have been selected to get typical thermodynamic conditions of a rocket engine cooling channel [34]. The propellants that are considered in the present study are cryogenic and will therefore typically enter the cooling system with a temperature slightly greater than the standard boiling temperature. More specifically, in the present numerical simulations, if T_{ev} is the standard boiling temperature, the assigned inlet temperature is $T_{\text{in}} = T_{\text{ev}} + 6K$.

The PNS solver used, together with the selected thermophysical models, has been verified by grid convergence analysis and validated by a comparison with experimental data: The validation and verification has been discussed in [18]. In particular, the grid convergence analysis carried out in [18], in conditions similar to those that are analyzed in the present work, permits one to select a suitable grid with a sufficient resolution for the numerical simulations of interest. The selected grid has 52 cells in the radial direction, which are clustered toward the wall to also describe the viscous sublayer. In fact, the height of the wall cell, in wall coordinates, is smaller than one ($y_w^+ < 1$). Because of the space-marching approach, the dimension of the step in the axial direction is determined by a numerical stability criterion and depends on the smallest cell in the radial direction and on local flow properties.

VI. Results

A. Methane, Ethane, and Propane

Heated channel flows of methane, ethane, and propane have been considered. The drop of the bulk total pressure along the channel, with respect to the inlet value, is shown in Fig. 5a. The pressure drop decreases, passing from methane to ethane to propane. The explanation is related to the fact that all the test cases have the same mass flow rate and so denser fluids enter the channel with a smaller velocity. Actually, propane is denser than ethane, which is denser than methane. For this reason, methane inlet velocity is $u_{\text{in}} = 20$ m/s, ethane velocity is $u_{\text{in}} = 15.48$ m/s, and propane velocity is $u_{\text{in}} = 14.45$ m/s. Moreover, heating yields a velocity increase, particularly for the methane cases. As a result, at the end of the channel, the relative total pressure drop is up to 50% greater for methane than for propane in the higher heat flux test case. It can therefore be deduced that, because reducing the pressure drops in the cooling channels is one of the design requirements, for the considered

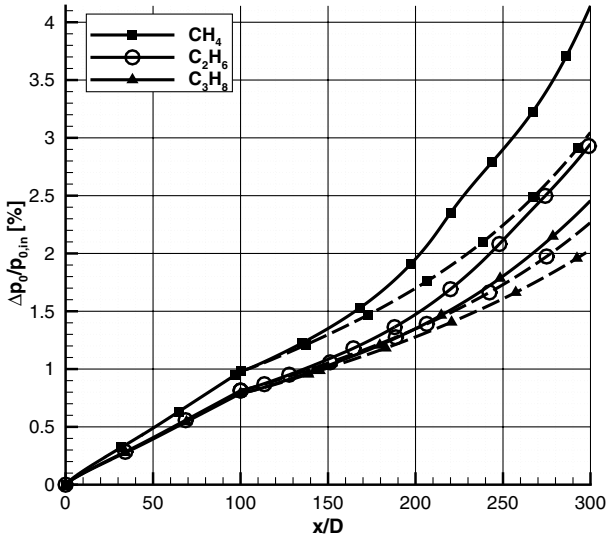

a) Bulk total pressure drop

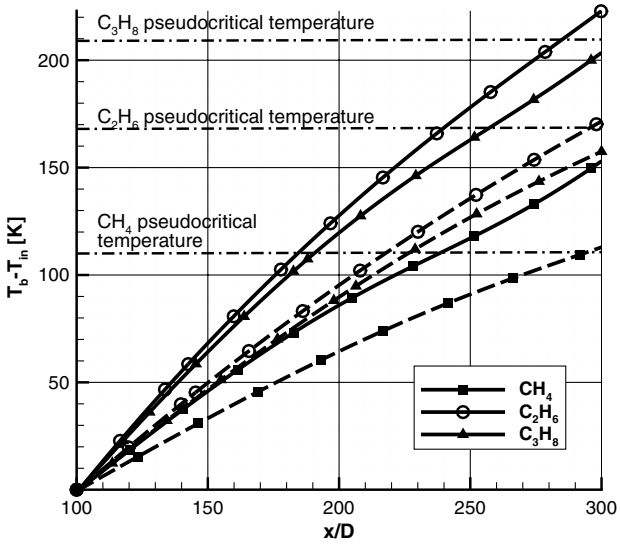

b) Bulk temperature increase

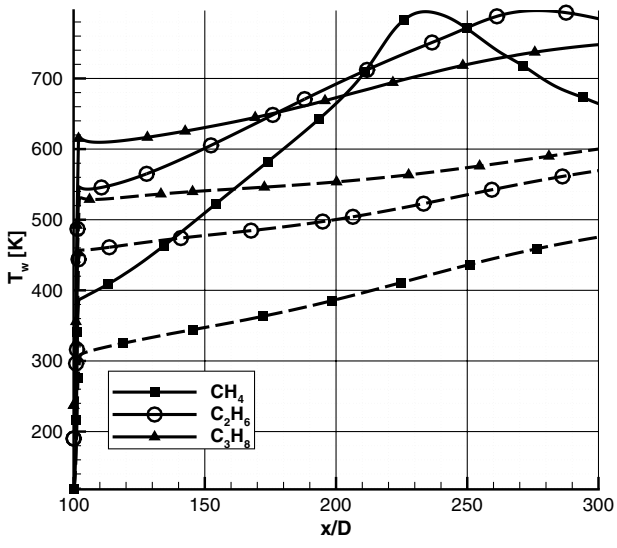

c) Wall temperature

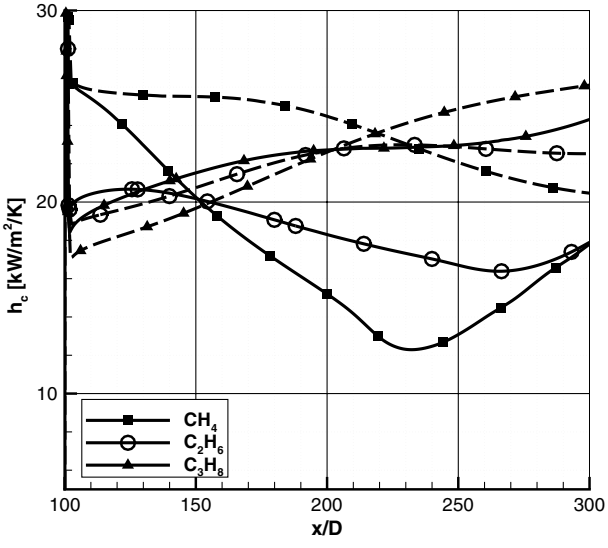

d) Convective heat transfer coefficient

Fig. 5 Heated channel flow of methane, ethane, and propane for $q_w = 5$ MW/m^2 (dashed lines) and $q_w = 7$ MW/m^2 (solid lines).

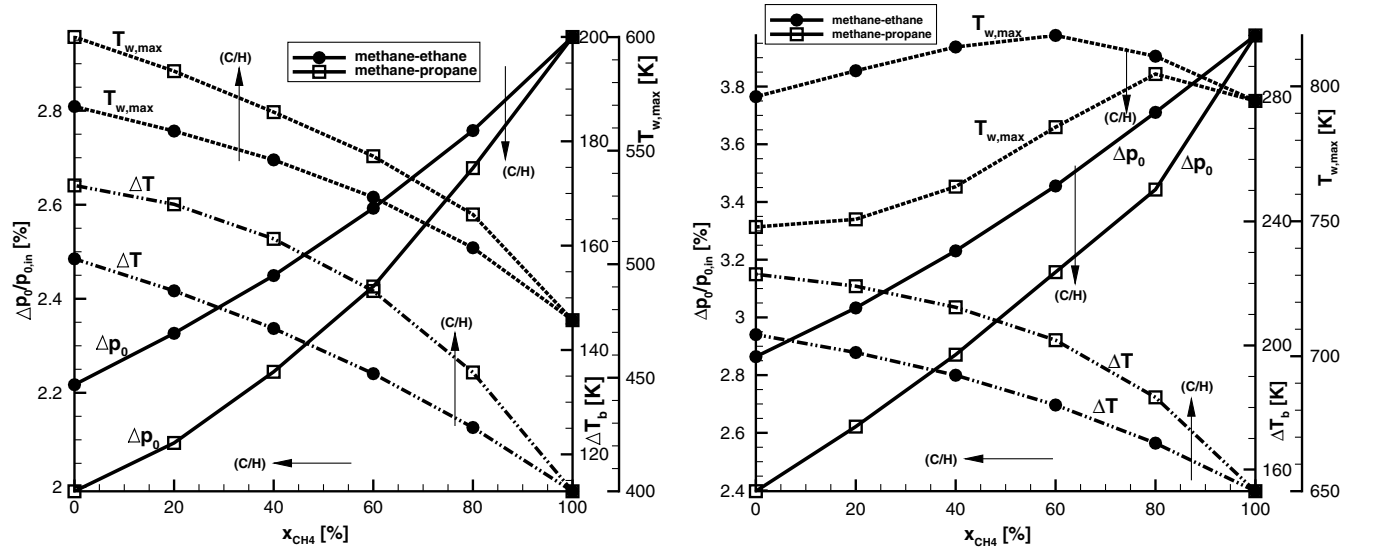

a) q_w=5 MW/m^2 b) q_w=7 MW/m^2

Fig. 6 Pressure drop, maximum wall temperature and exit bulk temperature for different binary mixtures.

conditions, propane would be favored with respect to ethane and methane, or a larger propane mass flow rate could be considered for the assigned channel dimension.

The bulk temperature difference $\Delta T = T_b - T_{\text{in}}$ and the wall temperature evolutions along the channel axis are reported in Figs. 5b and 5c. In the adiabatic part, not shown here, the temperatures can be considered constant. Moreover, for a given heat flux, being the mass flow rate assigned, the increase in the total enthalpy can also be considered as a fixed parameter of the analysis. As a consequence, different temperature increases in Fig. 5b can be related to differences in the thermodynamic and transport properties, which yield a different increase of static temperature and velocity for each propellant. For the present operative conditions, among the three propellants, methane shows to be the best coolant because, all along the channel, the increases in the bulk temperature are smaller than those for ethane and propane. Following the same reasoning, ethane would be favored with respect to propane.

The analysis of wall temperature requires one to observe that, dealing with forced convection heat transfer to supercritical pressure fluids in channels, the heat transfer can be either normal, enhanced, or deteriorated, depending on the heat flux level and on the fluid thermophysical characteristics [18,22,35–40].[‡] For the lower heat flux, a normal heat transfer occurs for the three propellants. In fact, analyzing first temperature and convective heat transfer coefficient h_c for the case of $q_w = 5$ MW/m^2, it can be noticed that wall temperature shows a monotonic increasing behavior (Fig. 5c). The heat transfer coefficient shows a different behavior for the three fuels: It is monotonically increasing for propane, whereas a light maximum is shown by ethane and a decreasing behavior is shown by methane (Fig. 5d). It is interesting to notice that, for the lower heat flux level, none of the flows undergo a pseudophase passage, because their exit temperatures are below or quite close to their pseudocritical value (see Fig. 5b, where emphasized are the pseudocritical values given by the specific heat peak in Fig. 3a and corresponding to $T_{\text{pc}} = 228$ K for methane, $T_{\text{pc}} = 358$ K for ethane, and $T_{\text{pc}} = 446$ K for propane). Therefore, the conditions of the flow at the end of the channels would not be suitable for a turbine expansion or, in other words, are not representative of the conditions at the cooling system outlet.

[‡]In the normal heat transfer mode, the values of the temperature field always increase in a monotonic trend as heat is enforced along the channel. Enhancement of heat transfer is characterized by a peak in the h_c. In the deteriorated mode, a thermal spike is present at a certain location along the channel. More precisely, the wall temperature exhibits a peak and, in the same axial location, the heat transfer coefficient h_c has a minimum value.

For the higher heat flux, $q_w = 7$ MW/m^2, deterioration occurs for methane and, at the very end of the channel, for ethane. This is shown by the peak of wall temperature in Fig. 5c, associated with a minimum of h_c (Fig. 5d). On the contrary, the behavior of wall temperature and heat transfer coefficient for propane is not different from the case of lower heat flux, therefore still showing a normal heat transfer. The fact that heat transfer deterioration occurs for methane and ethane but not for propane is due to their different thermophysical properties, which directly influence the threshold heat flux that a flow can bear without heat transfer deterioration [40]. As a consequence, propane has a higher heat transfer coefficient followed by ethane and methane, as can be observed in Fig. 5d. Despite the heat transfer deterioration, at the end of the channel, the lowest wall temperature is still that of the methane flow. Different from the case of $q_w = 5$ MW/m^2, in the higher heat flux case, bulk outlet temperature widely exceeds the pseudocritical value for methane and ethane, which means that, at the end of the channel, the flows are in supercritical gas-like conditions.

From the results that have been analyzed, it can be concluded that, in normal heat transfer conditions, methane is the best coolant. However, at high heat fluxes, when heat transfer deterioration occurs, methane shows a larger loss of cooling capability than propane and ethane. These results have been explained, considering the differences in thermophysical properties of the three propellants, as, for instance, the constant pressure specific heat and the molecular viscosity shown in Fig. 3 for $p = 13$ MPa, which is the inlet pressure of the channels.

B. Methane–Propane and Methane–Ethane Binary Mixtures

A behavior in between those of pure species can be expected in case of binary mixtures. In fact, in Fig. 3, the properties of the two binary mixtures, 50% methane–50% propane and 50% methane–50% ethane, are halfway between the corresponding pure species.

Binary mixtures of methane–propane and methane–ethane have therefore been considered. The composition of the binary mixtures is varied from one pure species to another. In each mixture, the methane percentage molar fraction is 0, 20, 40, 60, 80, or 100, and the remaining part is either ethane or propane. A useful parameter to describe the results is the ratio between the carbon and hydrogen content in the chemical compound, which will be indicated in the following with (C/H) [for instance, for methane $(C/H) = 0.25$].

The results obtained for the test case shown in Fig. 4 and the inlet temperature of the methane test case ($T_{\text{in}} = 118$ K) are summarized in Fig. 6, where the total pressure drop between the outlet and the inlet of the channel, the maximum wall temperature along the channel axis, and the difference between outlet and inlet bulk temperatures are reported against the methane molar fraction. Therefore, when reading

these figures, passing from left to right, the mixture composition varies from pure propane or pure ethane toward pure methane, and thus the (C/H) ratio decreases. For the same methane content, the (C/H) ratio increases, passing from ethane–methane to propane–ethane binary mixtures.

From these results, it comes out that the total pressure drop increases with the molar fraction, for both the heat fluxes. Moreover, for a same methane percentage, a greater pressure drop is found for the methane–ethane binary mixture than for the corresponding methane–propane one. Ultimately, it results that, when increasing the (C/H) ratio, the pressure loss decreases.

The ΔT has a monotonic behavior with the methane molar fraction and decreases when methane content increases. As for the simulation presented in the preceding section, the same total enthalpy increase can be associated with all the simulations. Therefore, differences in the bulk temperature increase are especially due to the differences in the constant pressure specific heat for varying composition. The c_p behavior at $p = 13$ MPa, shown in Fig. 3a, indicates that, at low and high temperatures, c_p increases with the (C/H) of the mixtures, whereas, in the 200–600 K temperature range, the curves cross with each other because of the pseudophase change, evidenced by the c_p peaks, which occur at different temperatures for the different fluids and mixtures. The bulk temperature values reached in the present simulations are such that methane has the greater specific heat, which explains why the exit temperature decreases with increasing methane molar fraction. For the same reason, being that propane c_p is lower than ethane, propane–methane mixtures undergo larger increases in the bulk temperature than ethane–methane binary mixtures.

The evolution of the maximum wall temperature $T_{w,\max}$ with the composition is different at $q_w = 5$ and $q_w = 7$ MW/m^2. For the lower heat flux, the $T_{w,\max}$ behavior is similar to the ΔT evolution, that is, it decreases with methane content. Conversely, for the higher heat flux, varying the binary mixture composition, $T_{w,\max}$ has a maximum at about 60% CH_4 for methane–ethane mixtures and 80% CH_4 for methane–propane mixtures. Moreover, for propane–methane binary mixtures, further decreasing the methane molar fraction decreases the $T_{w,\max}$ to smaller values than the pure methane case. The evolution of the wall temperature along the channel axis is shown in Fig. 7 for all the test cases. For the lower heat flux, wall temperature always increases along the channel, for all the mixtures, reaching the maximum value at the channel exit; differently, for the higher heat flux the wall temperature has a peak as a consequence of a heat transfer deterioration. The size and position of the peak varies with composition, because of the strong relation between heat transfer deterioration phenomena and thermophysical properties.

The heat transfer coefficient evolution along the axis shown in Fig. 8 is useful to observe the passage from the normal to deteriorated heat transfer, varying binary mixture composition. The pure methane test case is deteriorated and the heat transfer coefficient has, in fact, a minimum. Increasing the propane percentage, the h_c minimum in Fig. 8a becomes milder and milder, and for high propane contents, a monotonic increasing h_c is obtained, demonstrating a normal heat

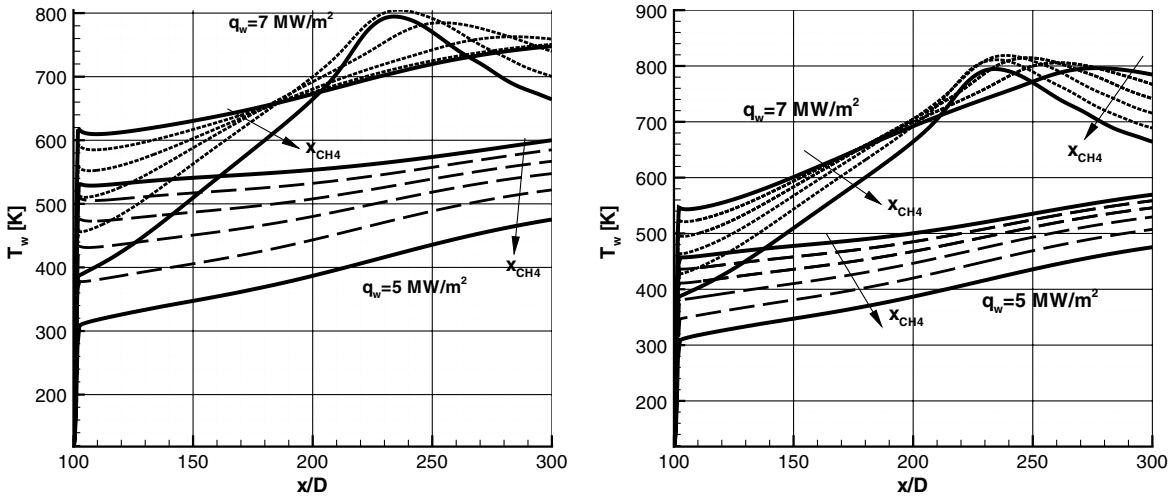

a) Methane-propane **b) Methane-ethane**

Fig. 7 Wall temperature for different binary mixtures methane–propane and methane–ethane, for $q_w = 5$ and $q_w = 7$ MW/m^2.

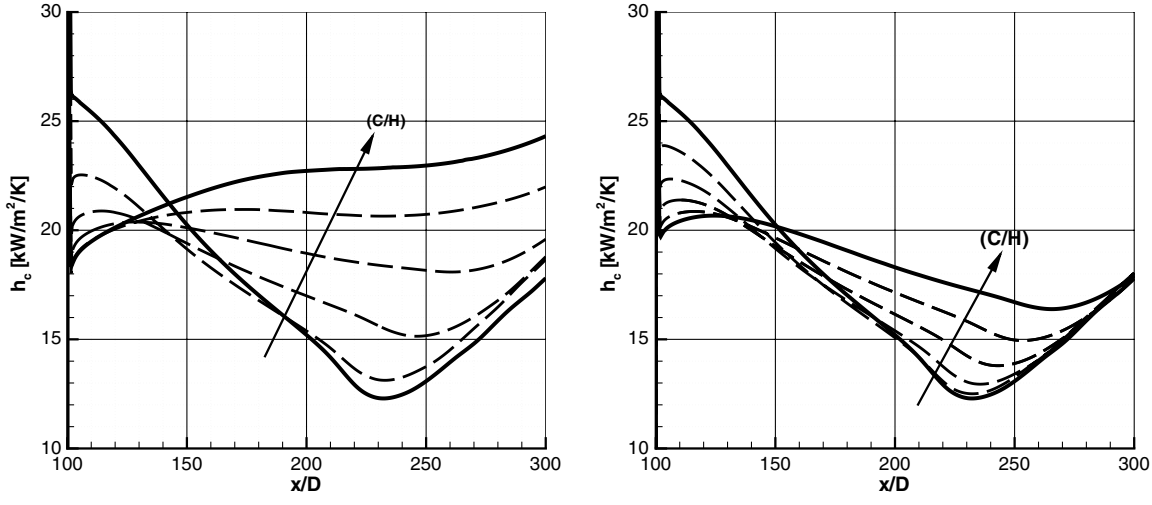

a) Methane-propane **b) Methane-ethane**

Fig. 8 Heat transfer coefficient for different binary mixtures, methane–propane and methane–ethane, for $q_w = 7$ MW/m^2.

Table 2 LNG composition range [3,41–47]

Species	Molar fraction, %
CH_4	80–99
C_2H_6	1–17
C_3H_8	0.1–5
C_4H_{10}	0.1–2
C_5H_{12} and heavier	≤1
N_2	0–5

Table 3 Molar fraction (in percentage) of the species in different LNG mixtures [3,41–47]

	CH_4	C_2H_6	C_3H_8	N_2
MIX1	92	4.0	2.2	1.8
MIX2	86	9.5	4.0	0.5
MIX3	93	5.0	1.5	0.5
MIX4	88	5.0	2.0	5.0

transfer mode. On the other hand, for ethane–methane binary mixture cases (Fig. 8b), heat transfer deterioration occurs for all the binary mixtures and, in fact, h_c reaches a minimum value for any percentage of methane.

C. Liquefied Natural Gas

LNG is a mixture of hydrocarbons and other components with a methane content usually greater than 90%. For this reason, methane and LNG are sometimes confused and LNG is also referred to as methane. Methane can be obtained from natural gas via purification processes. Anyway, LNG is more easily available because of its large common use in a multitude of fields and, being very similar to methane, it should have similar properties as a fuel for LRE

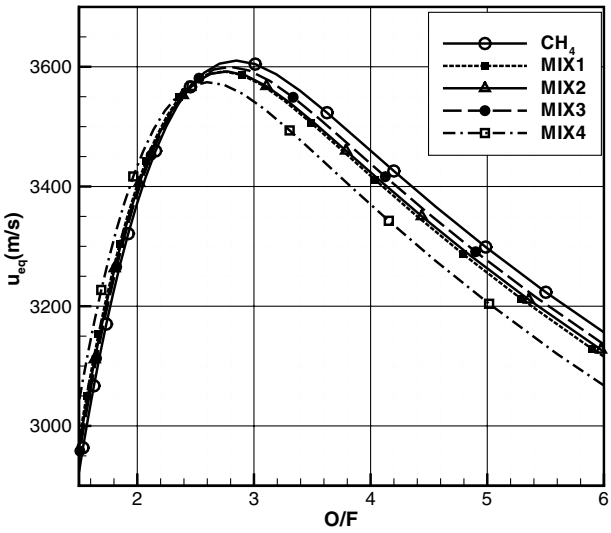

Fig. 9 Equivalent velocity vs oxidizer to fuel ratio for pure methane and LNG mixtures of Table 3.

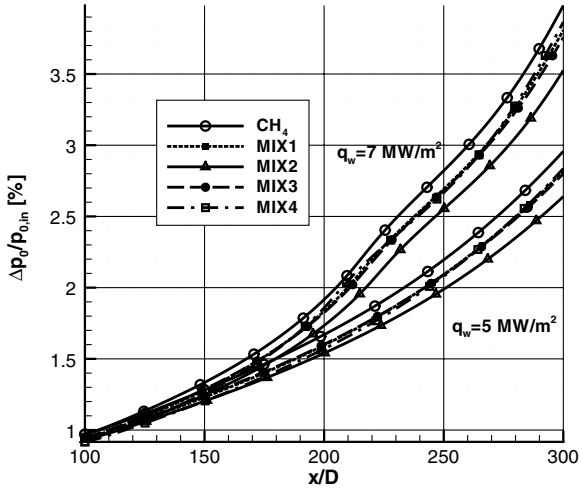

a) Bulk total pressure drop

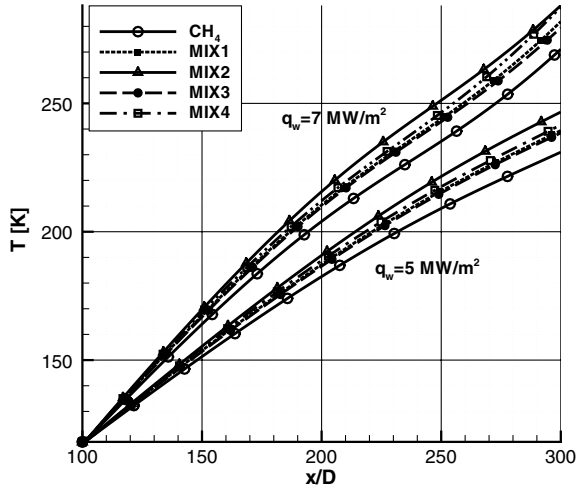

b) Bulk temperature

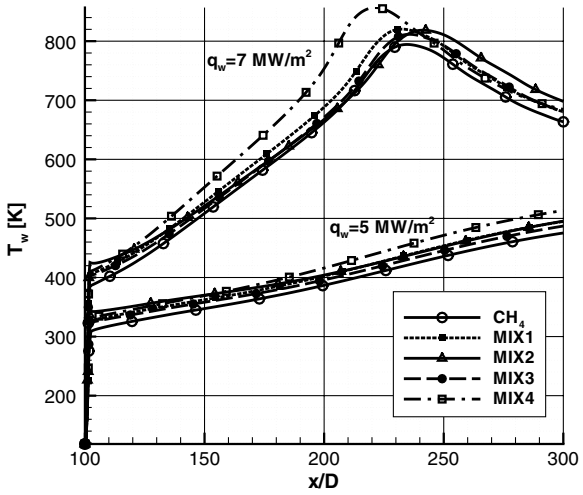

c) Wall temperature

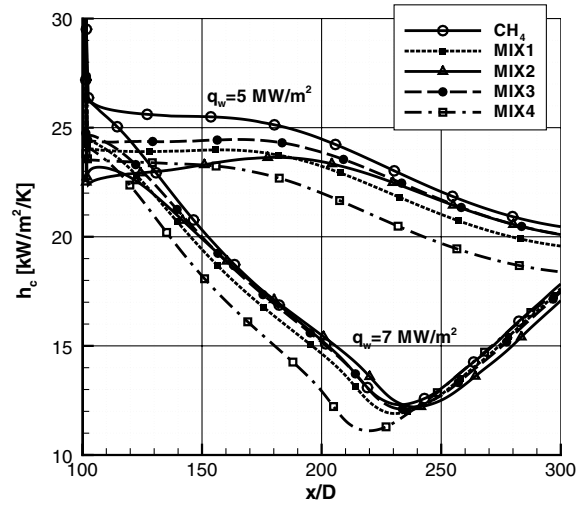

d) Convective heat transfer coefficient

Fig. 10 Heated channel flow with the different LNG compositions of Table 3.

applications. For this reason, it is interesting to consider also LNG in the present study on expander-cycle engine fuel candidates. The LNG composition depends on the quality specification and is quite variable around the world, but, in general, the molar fractions of the main components vary in the ranges reported in Table 2. In the present study, the heaviest hydrocarbon that has been considered is propane. Considering the ranges listed in Table 2, the compositions of Table 3 have been used for the numerical simulations.

A comparison of the equivalent velocity evolution with the (O/F) ratio is shown in Fig. 9 for the different considered LNG mixtures and pure methane to evaluate LNG/liquid oxygen engine performance. As expected, the curves are quite similar to each other, and differences in the u_{eq} values are smaller than 1%, showing that the performance is only slightly affected using LNG instead of pure methane as fuel.

Numerical computation of heated channel flows, for the test case of Fig. 4, are carried out considering the four different mixtures of Table 3. The results obtained for both the investigated heat fluxes (5 and 7 MW/m^2) are shown in Fig. 10. The drop of the bulk total pressure with respect to the inlet total pressure is shown in Fig. 10a. Higher heat flux yields larger pressure drops, as could be expected. On the other hand, for each heat flux, the curves are similar for all the LNG compositions, but the values are slightly different. The greater total drop is found for the methane case, whereas the drops for the LNG mixtures cases are 5–10% smaller, for both the heat fluxes, according to the results obtained for binary mixtures obtained in the foregoing section. In Figs. 10b and 10c, among the investigated mixtures, the smaller increase in the bulk temperature is found for methane, mainly because of its greater c_p. In fact, bulk temperature for the LNG compositions are 3–7% greater than for pure methane (Fig. 10b). Also, the wall temperature is smaller for pure methane: At the channel exit, the LNG wall temperature is 4–8% greater than the methane one (Fig. 10c). The h_c curves show that, among the investigated compositions, the pure methane case always has the greatest h_c along the channel: It can be concluded that, in the present conditions, the heat transfer efficiency decreases, passing from pure methane to LNG (Fig. 10d). For the highest heat flux, a deterioration of the heat transfer occurs. In fact, the wall temperature has a peak that corresponds with a minimum in the heat transfer coefficient. From a quantitative point of view, the percentage differences between pure methane and LNG mixtures are of the same order of magnitude as those observed for the normal heat transfer case ($q_w = 5\ \text{MW}/\text{m}^2$). Namely, the differences are up to 8% for the temperatures. Despite that, it has to be considered that, in the wall temperature peak region, an increment of 8% could be important in terms of absolute values. As can be observed in Fig. 10c, the difference in the peak value of the wall temperature is up to 60 K between pure methane and LNG. It is finally worth emphasizing that the presence of heavier hydrocarbons forces the maximum allowable temperature to lower values than pure methane because of the possible occurrence of coking, which could occur, for instance, at the peak temperature of Fig. 10c.

VII. Conclusions

The study of cooling properties of candidate expander-cycle fuels for liquid rocket engines, like methane, ethane, propane, binary mixtures of them, and natural gas, has been carried out by the comparison of flow and wall temperature evolution in a single straight heated tube, with the same inlet pressure, mass flow rate, and temperature slightly higher than the evaporation temperature. All examined fuels are good candidates as expander-cycle fuels in terms of performance, showing only slightly different values of theoretically reachable chamber pressure and exhaust velocity. The parametric analysis of fuel heating in channels has shown some differences among fuels in terms of pressure losses and wall temperatures. A general result is that, increasing the carbon to hydrogen ratio (C/H), the total pressure drop along the channel decreases. On the contrary, different behaviors are observed for the heat transfer capability and wall temperature depending on the heat flux level. For low heat fluxes, for which the heat transfer is normal for all the considered mixtures and fluids, the cooling capabilities decrease when increasing the (C/H) ratio. For high heat fluxes, a pseudophase passage occurs, which may lead to a heat transfer deterioration and thus to a loss of cooling capability. Deterioration is evident for methane, ethane, and their mixtures, including natural gas. An interesting result is that the temperature peak is not maximum for pure methane but in the presence of a significant amount of ethane or propane. Selected mixtures representative of natural gas behave accordingly, resulting in a possible enhancement of the temperature peak, which has to be considered together with a lower admissible maximum temperature due to the constraint of avoiding coking by the heavier hydrocarbons.

Acknowledgment

Partial funding by the Italian Ministry for Education, University, and Research is acknowledged.

References

[1] Parsley, R. C., and Zhang, B., "Thermodynamic Power Cycles for Pump-Fed Liquid Rocket Engines," *Liquid Rocket Thrust Chambers: Aspects of Modeling, Analysis, and Design*, edited by Yang, V., Habiballah, M., Popp, M., and Hulka, J., Vol. 200, Progress in Astronautics and Aeronautics, AIAA, Reston, VA, 2004, pp. 621–648.

[2] Manski, D., Goertz, C., Saßnick, H.-D., Hulka, J. R., Goracke, B. D., and Levack, D. J. H., "Cycles for Earth-to-Orbit Propulsion," *Journal of Propulsion and Power*, Vol. 14, No. 5, 1998, pp. 588–604. doi:10.2514/2.5351

[3] Han, P.-G., Lee, S.-W., Kim, K.-H., and Yoon, Y., "Performance Analysis of the Thrust Chamber in Liquid Rocket Engine using Liquefied Natural Gas as a Fuel," *40th AIAA/ASME/SAE/ASEE Joint Propulsion Conference and Exhibit*, AIAA Paper 2004-3860, 2004.

[4] Noguchi, Y., Taya, K., Hirai, T., Yui, A., and Makino, T., "Conceptual Design of a LOX/LNG Rocket Engine for a Space Tourism Vehicle," *45th AIAA/ASME/SAE/ASEE Joint Propulsion Conference and Exhibit*, AIAA Paper 2009-5138, 2009.

[5] Higashino, K., Sugioka, M., Kobayashi, T., Minato, R., Maru, Y., Sasayama, Y., Otsuka, M., Makino, T., and Sakaguchi, H., "Fundamental Study on Coking Characteristics of LNG Rocket Engines," *44th AIAA/ASME/SAE/ASEE Joint Propulsion Conference and Exhibit*, AIAA Paper 2008-4753, 2008.

[6] Urbano, A., and Nasuti, F., "Numerical Analysis of Heated Channel Flows by a Space-Marching Finite-Volume Technique," *Journal of Thermophysics and Heat Transfer*, Vol. 25, No. 2, 2011, pp. 282–290. doi:10.2514/1.51741

[7] Urbano, A., and Nasuti, F., "An approximate Riemann Solver for Real Gas Parabolized Navier–Stokes Equations," *Journal of Computational Physics*, Vol. 233, Jan. 2013, pp. 574–591. doi:10.1016/j.jcp.2012.09.019

[8] Kunz, O., Klimeck, R., Wagner, W., and Jaeschke, M., "The GERG-2004 Wide-Range Equation of State for Natural Gases and Other Mixtures," Groupe Européen de Recherches Gazières TR-TM15, 2007.

[9] Huber, M. L., Laesecke, A., and Perkins, R. A., "Model for the Viscosity and Thermal Conductivity of Refrigerants, Including a New Correlation for the Viscosity of R134a," *Industrial & Engineering Chemistry Research*, Vol. 42, No. 13, 2003, pp. 3163–3178. doi:10.1021/ie0300880

[10] Klein, S. A., McLinden, M. O., and Laesecke, A., "An Improved Extended Corresponding States Method for Estimation of Viscosity of Pure Refrigerants and Mixtures," *International Journal of Refrigeration*, Vol. 20, No. 3, 1997, pp. 208–217. doi:10.1016/S0140-7007(96)00073-4

[11] Liang, K., Yang, B., and Zhang, Z., "Investigation of Heat Transfer and Coking Characteristics of Hydrocarbon Fuels," *Journal of Propulsion and Power*, Vol. 14, No. 5, 1998, pp. 789–796. doi:10.2514/2.5342

[12] Mitchell, J., and Gregory, J., "Space Storable Regenerative Cooling Investigation," NASA CR-72341, 1968.

[13] Haeseler, D., Mäding, C., Götz, A., Roubinski, V., Khrissanfov, S., and Berejnoy, V., "Recent Developments for Future Launch Vehicle LOX/HC Rocket Engines," *6th International Symposium Propulsion for Space Transportation of the XXI Century*, Association Aéronautique et Astronautique de France Paper 02-100, 2012.

[14] McBride, B. J., and Gordon, S., "Computer Program for Calculation of Complex Chemical Equilibrium Compositions and Applications I: Analysis," NASA Lewis Research Center, Reference Publ. NASA, RP-1311, Oct. 1994.

[15] McBride, B., and Gordon, S., "Computer Program for Calculation of Complex Chemical Equilibrium Compositions and Applications II: User's Manual and Program Description," NASA Lewis Research Center, Reference Publ. NASA RP-1311, June 1996.

[16] Sutton, G. P., "History of Liquid Propellant Rocket Engines in the United States," *Journal of Propulsion and Power*, Vol. 19, No. 6, 2003, pp. 978–1007. doi:10.2514/2.6942

[17] Sackheim, R. L., "Overview of United States Rocket Propulsion Technology and Associated Space Transportation Systems," *Journal of Propulsion and Power*, Vol. 22, No. 6, 2006, pp. 1310–1332. doi:10.2514/1.23257

[18] Urbano, A., and Nasuti, F., "Parametric Analysis of Heat Transfer to Supercritical-Pressure Methane," *Journal of Thermophysics and Heat Transfer*, Vol. 26, No. 3, July–Sept. 2012, pp. 450–463. doi:10.2514/1.T3840

[19] Spalart, P., and Allmaras, S., "A One-Equation Turbulence Model for Aerodynamic Flow," *La Recherche Aerospatiale*, Vol. 1, 1994, pp. 5–21.

[20] Roe, P., "Approximate Riemann Solvers, Parameter Vectors, and Difference Schemes," *Journal of Computational Physics*, Vol. 43, No. 2, 1981, pp. 357–372. doi:10.1016/0021-9991(81)90128-5

[21] Urbano, A., and Nasuti, F., "Numerical Study of Liquefied Natural Gas as a Coolant in Liquid Rocket Engines," *Proceedings of the Institution of Mechanical Engineers, Part G: Journal of Aerospace Engineering*, 2013. doi:10.1177/0954410012451376.

[22] Urbano, A., and Nasuti, F., "Onset of Heat Transfer Deterioration in Supercritical Methane Flow Channels," *Journal of Thermophysics and Heat Transfer*, Vol. 27, No. 2, 2013, pp. 298–308. doi:10.2514/1.T4001

[23] Boushehri, A., Bzowski, J., Kestin, J., and Mason, E., "Equilibrium and Transport Properties of Eleven Polyatomic Gases at Low Density," *Journal of Physical and Chemical Reference Data*, Vol. 16, No. 3, 1987, pp. 445–467. doi:10.1063/1.555800

[24] Svehla, R., "Transport Coefficients for the Nasa Lewis Chemical Equilibrium Program," NASA TM-4647, 1995.

[25] Vogel, E., Kuchenmeister, C., and Bich, E., "Reference Correlation of the Viscosity of Propane," *Journal of Physical and Chemical Reference Data*, Vol. 27, No. 5, 1998, pp. 947–955. doi:10.1063/1.556025

[26] Marsh, K., Perkins, R., and Ramires, M., "Measurement and Correlation of the Thermal Conductivity of Propane from 86 K to 600 K at Pressures to 70 MPa," *Journal of Chemical and Engineering Data*, Vol. 47, No. 4, 2002, pp. 932–940. doi:10.1021/je010001m

[27] Quinones-Cisneros, S. E., and Deiters, U. K., "Generalization of the Friction Theory for Viscosity Modeling," *Journal of Physical Chemistry B*, Vol. 110, No. 25, 2006, pp. 12820–12834. doi:10.1021/jp0618577

[28] Friend, D., Ely, J., and Ingham, H., "Thermophysical Properties of Methane," *Journal of Physical and Chemical Reference Data*, Vol. 18, No. 2, 1989, pp. 583–638. doi:10.1063/1.555828

[29] Lemmon, E., and Jacobsen, R., "Viscosity and Thermal Conductivity Equations for Nitrogen, Oxygen, Argon, and Air," *International Journal of Thermophysics*, Vol. 25, No. 1, 2003, pp. 21–69.

[30] Friend, D., Ingham, H., and Ely, J., "Thermophysical Properties of Ethane," *Journal of Physical and Chemical Reference Data*, Vol. 20, No. 2, 1991, pp. 275–347. doi:10.1063/1.555881

[31] Lemmon, E., and Jacobsen, R., "Viscosity and Thermal Conductivity Equations for Nitrogen, Oxygen, Argon, and Air," *International Journal of Thermophysics*, Vol. 25, No. 1, 2003, pp. 21–69. doi:10.1023/B:IJOT.0000022327.04529.f3

[32] Olchowy, G., and Sengers, J., "A Simplified Representation for the Thermal Conductivity of Fluids in the Critical Region," *International Journal of Thermophysics*, Vol. 10, No. 2, 1989, pp. 417–426. doi:10.1007/BF01133538

[33] Di Matteo, F., De Rosa, M., and Onofri, M., "Start-Up Transient Simulation of a Liquid Rocket Engine," *47th AIAA/ASME/SAE/ASEE Joint Propulsion Conference*, AIAA Paper 2011-6032, Aug. 2011.

[34] Schuff, R., Mayer, M., Sindiy, O., Ulrich, C., and Fugger, S., "Integrated Modeling and Analysis for a LOX/Methane Expander Cycle Engine: Focusing on Regenerative Cooling Jacket Design," *42nd AIAA/ASME/SAE/ASEE Joint Propulsion Conference*, AIAA Paper 2006-4534, July 2006.

[35] Kelbaliev, R., "Deterioration of Heat Transfer at Supercritical Pressures of a Substance," *Journal of Engineering Physics and Thermophysics*, Vol. 74, No. 2, 2001, pp. 416–420. doi:10.1023/A:1016621009439

[36] Yamashita, T., Mori, H., Yoshida, S., and Ohno, M., "Heat Transfer and Pressure Drop of a Supercritical Pressure Fluid Flowing in a Tube of Small Diameter," *Memoirs of the Faculty of Engineering, Kyushu University*, Vol. 63, No. 4, 2003, pp. 227–244.

[37] Pioro, I., and Duffey, R., "Experimental Heat Transfer in Supercritical Water Flowing Inside Channels (Survey)," *Nuclear Engineering and Design*, Vol. 235, No. 22, 2005, pp. 2407–2430. doi:10.1016/j.nucengdes.2005.05.034

[38] Pizzarelli, M., Urbano, A., and Nasuti, F., "Numerical Analysis of Deterioration in Heat Transfer to Near-Critical Rocket Propellants," *Numerical Heat Transfer, Part A: Applications*, Vol. 57, No. 5, 2010, pp. 297–314. doi:10.1080/10407780903583016

[39] Grabezhnaya, V. A., and Kirillov, P. L., "Heat-Transfer Degradation Boundary in Supercritical-Pressure Flow," *Atomic Energy*, Vol. 101, No. 4, 2006, pp. 714–721. doi:10.1007/s10512-006-0158-5

[40] Urbano, A., and Nasuti, F., "Boundaries for Heat Transfer Deterioration Onset in Supercritical Pressure Channel Flows," *ECCOMAS 2012 — European Congress on Computational Methods in Applied Sciences and Engineering, e-Book Full Papers*, ECCOMAS, Barcelona, Spain, 2012, pp. 3138–3157.

[41] Domaschenko, A., Dovbish, A., Darbinyan, R., Lyapin, A., and Peredle'skii, V., "Analysis of Liquefied Methane Production Technology Depending on Methane Purity and Production Volume," *Journal of Petroleum Science and Engineering*, Vol. 40, No. 3, 2004, pp. 145–148. doi:10.1023/B:CAPE.0000033665.68451.1c

[42] Querol, E., Gonzalez-Regueral, B., García-Torrent, J., and Ramos, A., "Available Power Generation Cycles to be Coupled with the Liquid Natural Gas (LNG) Vaporization Process in a Spanish LNG Terminal," *Applied Energy*, Vol. 88, No. 7, 2011, pp. 2382–2390. doi:10.1016/j.apenergy.2011.01.023

[43] Hissong, D., "Keys to Modeling LNG Spills on Water," *Journal of Hazardous Materials*, Vol. 140, No. 3, 2007, pp. 465–477. doi:10.1016/j.jhazmat.2006.10.040

[44] "LNG Interchangeability/Gas Quality: Results of the National Energy Technology Laboratory's Research for the FERC on Natural Gas Quality and Interchangeability," U.S. Dept. of Energy National Energy Technology Lab. Rept., 2007.

[45] Conrado, C., and Vesovic, V., "The Influence of Chemical Composition on Vaporisation of LNG and LPG on Unconfined Water Surfaces," *Chemical Engineering Science*, Vol. 55, No. 20, 2000, pp. 4549–4562. doi:10.1016/S0009-2509(00)00110-X

[46] Nasrifar, K., and Bolland, O., "Prediction of Thermodynamic Properties of Natural Gas Mixtures Using 10 Equations of State Including a New Cubic Two-Constant Equation of State," *Journal of Petroleum Science and Engineering*, Vol. 51, Nos. 3–4, 2006, pp. 253–266. doi:10.1016/j.petrol.2006.01.004

[47] Cook, R., "Methane Heat Transfer Investigation," NASA, CR-171051, June 1984.

J. Oefelein
Associate Editor